Spectrum of scandium in the energy region 52 625–54 046 cm^{-1}

Feng-Dong Jia,[1] Zhi-Ping Zhong,[1,*] Wei Sun,[2] Ping Xue,[2] and Xiang-Yuan Xu[2,3]
[1]*College of Physical Sciences, Graduate University of the Chinese Academy of Sciences, P.O. Box 4588, Beijing 100049, China*
[2]*Department of Physics, The Key Laboratory of Atomic and Molecular Nanosciences of the Ministry of Education, Tsinghua University, Beijing 100084, China*
[3]*Department of Physics, Capital Normal University, P.O. Box 8009, Beijing 100088, China*
(Received 28 December 2008; published 6 March 2009)

The Rydberg and autoionization Rydberg spectrum of scandium via intermediate state [Ar] $3d4s4p\ ^2F_{5/2}$ have been measured in the energy region 52 625–54 046 cm^{-1} using two-laser resonance excitation. Four autoionization Rydberg series are observed. Eigenquantum defects μ_α and transformation matrices $U_{i\alpha}$ are calculated from first principles by relativistic multichannel theory within the framework of multichannel quantum defect theory, while the dipole matrix elements D_α are obtained by comparing with experimental data. With these parameters μ_α, $U_{i\alpha}$ and D_α, Rydberg and autoionization Rydberg spectrum of scandium are calculated and the experimental peaks are then clearly assigned. More specifically, one autoionization Rydberg series is converged to $Sc^+\ 3d4s\ ^3D_3$, the other three series are converged to $Sc^+\ 3d4s\ ^1D_2$, and one autoionization state converging to $Sc^+\ 3d^2(^3F_2)$ and/or $Sc^+\ 3d^2(^1D_2)$ are assigned. In addition, the Fano parameters E_r, q, and Γ for some of these states are fitted and analyzed.

DOI: 10.1103/PhysRevA.79.032505 PACS number(s): 31.15.vj, 32.70.−n, 32.80.Rm

I. INTRODUCTION

The investigation of electron-electron correlations of atoms is a significant subject in atomic physics research. Atomic scandium (Sc) [Ar] $3d4s^2$ has three valence electrons and is the simplest open-shell atom with a partially field d subshell, and can show complex spectra. In fact, the first 13 levels of Sc^+ are spread across only 14 000 cm^{-1} (1.7 eV) [1]; the small spread is partly due to the near degeneracy of the $4s$ and $3d$ orbitals. Consequently, there are rich and complex energy structures in the valence excitation spectrum of Sc. Therefore, Sc can be employed to demonstrate rich electron-electron correlation effects. On the other hand, as the simplest rare-earth-metal element, the lessons learned from scandium may apply to other rare-earth-metal elements since the valence shells for all these atoms include both s and d orbitals [2]. While rare-earth-metal elements are now widely used in material industry [3,4], understanding of the electronic structure of rare-earth-metal elements would benefit the applications in relative industries. These make scandium especially attractive from both theoretical and experimental points of view.

There has been a continuous effort on the spectrum of scandium in terms of experimental and theoretical investigation. The present work focus on the valence excitation spectrum, which would exhibit complex energy structures and then rich electron-electron correlation effects as discussed above. Reference [1] has summarized the previous experimental work, and eight odd-parity Rydberg and autoionization Rydberg series related to the excitation of a $3d$ or $4s$ excitation are observed by Garton *et al.* [5], i.e., $4s^2(^1S)nf\ ^2F^o_{5/2,7/2}$, $3d4s(^1D)np\ ^2P^o_{1/2,3/2}$, $3d4s(^1D)np\ ^2D^o_{3/2,5/2}$, and $3d^2(^3F)np\ ^2F^o$. Theoretically, based on eigenchannel R-matrix calculations, Robicheaux and Greene [2] have calculated the photoionization odd-parity spectrum of Sc to classify most of the autoionizing lines reported by Garton *et al.* [5]. It should be noted that the techniques employed by Robicheaux and Greene [2] are "nearly" *ab initio*, i.e., the effects of the 18 core electrons are described using a screened Coulomb potential [6,7] with a dipole polarizability, and spin-orbit effects are incorporated through the $LS-jj$ frame transformation [8,9]. The difference between their calculated and experimental quantum defects is generally smaller than 0.03. Recently, we have calculated autoionization Rydberg series $4s^2nf\ ^2F^o_{7/2}$ [10], $3d4s(^1D)np\ ^2D^o_{3/2,5/2}$, $3d4s(^1D)np\ ^2P^o_{1/2,3/2}$ [11] of scandium from first principles by relativistic multichannel theory (RMCT) within the framework of multichannel quantum defect theory (MQDT), the difference between calculated and experimental quantum defects is generally smaller than 0.03. Meanwhile, we have measured the experimental even-parity spectrum of Sc via intermediate state [Ar] $3d4s4p\ ^2F_{5/2}$ in the energy range 52 625–54 046 cm^{-1} with two-laser resonance excitation. Therefore, we can classify the experimental spectrum from first principles by RMCT within the framework of MQDT. This paper is organized as follows. In Sec. II, we briefly describe the present experimental and theoretical method. In Sec. III, we present our experimental spectrum and calculated eigenchannel spectrum. The comparison between them and discussions are also given. In the conclusion, we summarize the assignments for the experimental peaks.

II. EXPERIMENTAL METHOD AND THEORETICAL METHOD

A. Experimental method

The experimental setup has been in detail described in Ref. [12]. Briefly, scandium atoms originating from a heated crucible in a vacuum chamber are excited from the ground

*zpzhong@gucas.ac.cn

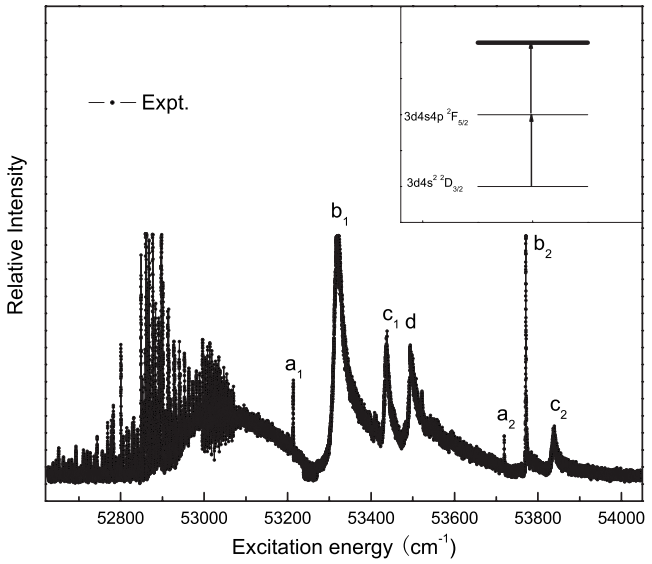

FIG. 1. Experimental spectrum of Sc Rydberg and autoionization states via intermediate state Sc [Ar] $3d4s4p\ ^2F_{5/2}$ in the energy region 52 625–54 046 cm^{-1}. The ionization thresholds are taken from Ref. [1]. The inset displays the excitation scheme of Sc in this work.

state [Ar] $3d4s^2\ ^2D_{3/2}$ to excited states via intermediate state $3d4s4p\ ^2F_{5/2}$ by two-laser resonance excitation. More specifically, the scandium atoms are excited to the intermediate state $3d4s4p\ ^2F_{5/2}$ by the first laser, then the second laser is scanned near the scandium ionization thresholds to excite the Rydberg and autoionization Rydberg states. The two dye lasers pumped by an XeCl excimer laser are used in this experiment with about 0.5 cm^{-1} linewidth. Shortly after the laser excitation, Sc atoms in highly excited states are converted to Sc^+ ions by a pulsed electrical field. These ions are extracted through a field-free zone into a cell where a strong constant electric field exists. Lastly the ions are detected by a microchannel plate detector with a time-of-flight mass spectrometer. Figure 1 displays the experimental spectrum which spans the lowest three ionization thresholds of Sc and in the energy region 52 625–54 046 cm^{-1} above the ground state $3d4s^2\ ^2D_{3/2}$.

B. Theoretical method

Within the framework of MQDT [9,13–18], infinite Rydberg states and adjacent continua states can be treated in a unified manner through a compact set of physical MQDT parameters (eigenquantum defects μ_α, transformation matrices $U_{i\alpha}$, and dipole matrix elements D_α). These MQDT parameters (eigenquantum defects μ_α, transformation matrices $U_{i\alpha}$, and dipole matrix elements D_α) are smoothly energy dependent within the neighborhood of a threshold. This is the so-called eigenchannel characters. They can be determined semiempirically by fitting accurate energy levels into spectroscopic data or by the first-principles calculations. However, the numerical fitting procedure requires rather complete spectroscopic data, which is always a difficult and tedious task with the increasing number of related channels, thus it confines the scope of application of MQDT. In a few cases, the MQDT parameters $(\mu_\alpha, U_{i\alpha})$ can be calculated from first principles with the nonrelativistic theory [9,19]. The RMCT can be regarded as an extension of the traditional configuration interaction method by including the continuum configuration interactions [20–26]. It aims directly to calculate the MQDT parameters $(\mu_\alpha, U_{i\alpha})$ and has been used to calculate atomic energy levels, Lande g factors, and the coupling scheme within the framework of the MQDT [21–26].

Since the detailed description of the RMCT has been given elsewhere [20–26], here we only give an outline. We start with a relativistic atomic Hamiltonian H that is obtained by adopting the Coulomb gauge, namely,

$$H\Psi = E\Psi. \tag{1}$$

With the relativistic atomic Hamiltonian

$$H = \sum_i^n \left(c\alpha_i P_i + \beta_i mc^2 - \frac{Ze^2}{r_i} \right) + \sum_{i>j} \frac{e^2}{r_{ij}} = H_0 + V, \tag{2}$$

here H_0 is a relativistic self-consistent field (SCF) atomic Hamiltonian and V is a residual interaction. The Breit interactions and the rest of the higher-order quantum electrodynamic interactions are not included and can be treated as perturbations later. Based on the relativistic atomic self-consistent field potential V_{SCF} obtained by the Dirac-Slater SCF method, bound and continuum single-electron wave functions are calculated.

From such a complete set of single-electron wave functions, i.e., orbital wave functions of energy eigenstates can be expressed as the superposition of bound and continuum configuration wave functions (Φ_n and $\Phi_{j\varepsilon}$) [20–26],

$$\Psi(E,i) = \sum_n A_n(E,i)\phi_n + \sum_j \int_{\varepsilon_c} B_{j\varepsilon}(E,i)\Phi_{j\varepsilon} d\varepsilon, \tag{3}$$

where the index j refers to various dissociation channels. $A_n(E,i)$ and $B_{j\varepsilon}(E,i)$ are the coefficients of linear superposition. With the calculated matrix elements of residual interactions $V_{n,n'}$, $V_{n,j\varepsilon}$, and $V_{j\varepsilon,j'\varepsilon'}$ (representing discrete-discrete, discrete-continuum, and continuum-continuum interactions, respectively), it then leads to Lippmann-Schwinger integral equations of the K matrix at $E \geq \varepsilon_c$; the physical parameters (eigenquantum defects μ_α and transformation matrix $U_{i\alpha}$) in MQDT can be obtained directly by diagonalizing the K matrix on energy shell [20–26]. In the autoionization region, μ_α and $U_{i\alpha}$ are related as

$$\begin{aligned} \mathrm{Det}|F_{i\alpha}| &= \mathrm{Det}|U_{i\alpha} \sin[\pi(x_i + \mu_\alpha)]| \\ &= 0 \begin{cases} \text{for } x_i = \nu_i & i \in \bar{Q}, \\ \text{for } x_i = -\tau_\rho & i \in \bar{P}. \end{cases} \end{aligned} \tag{4}$$

For the closed dissociation channels ($i \in \bar{Q}$), ν_i is the effective quantum number of the ith channel. Each collision eigenstate ρ being a superposition of the standing waves of open dissociation channels ($i \in \bar{P}$) with the same eigenphase shift $\pi\rho$. The reduced dipole matrix element from the initial state to the ρth autoionization channel can be written as [18]

$$\mathcal{D}_\rho = \sum_\alpha D_\alpha A_\alpha^\rho + D_{cc,\rho}, \tag{5}$$

where D_α is the dipole matrix element for the channel excitation and $D_{cc,\rho}$ is the matrix element for core excitation. A_α^ρ is the mixing coefficient as functions of μ_α and $U_{i\alpha}$.

In the energy region of interest, the spectrum is far away from the core excitation, thus

$$\mathcal{D}_\rho \sim \sum_\alpha D_\alpha A_\alpha^\rho. \tag{6}$$

Then the scattering cross sections are [13,9,15,17,18]

$$\sigma = 2\pi^2 \alpha a_0^2 (df/d\varepsilon) = 4\pi^2 \alpha a_0^2 \omega \sum_\rho \mathcal{D}_\rho^2 = \sum_\rho \left(\sum_\alpha D_\alpha A_\alpha^\rho \right)^2, \tag{7}$$

where $(df/d\varepsilon)$ is the density of oscillator strengths, α is the fine structure constant, a_0=0.529 Å, and ω is the photon energy in a.u..

Due to eigenchannel characters, we only calculate MQDT parameters at a few energy points across the threshold, then these MQDT parameters at any energy point within the neighborhood of threshold can be obtained by interpolating or extrapolating from the calculated data. As for the dipole matrix elements D_α, they can be assumed as constants within the energy region of interest. According to Eq. (7), the observed autoionization states can be obtained from the mixing of different autoionization channels ρ and then different eigenchannels α. Usually, if one specific peak in the experimental spectrum mainly comes from one eigenchannel, the peak can be assigned as an autoionization state belonging to this eigenchannel. Similar to the work of reference [27,28], we did the assignment as follows: first we calculated the eigenchannel spectrum for a specific eigenchannel α by setting $D_{\alpha'} = \delta_{\alpha\alpha'}$ [27,28]. Then compare this eigenchannel spectrum with the experimental spectrum in terms of energy position to assign specific peaks. Clearly, this eigenchannel spectrum may not correctly reflect the profile for a specific peak, especially for the strongly perturbed resonance, but it can meet the purpose of assignment in normal cases. In fact, the spectrum mixing of different eigenchannel spectrum Eq. (7) may be different from a specific eigenchannel spectrum in terms of energy position and width.

III. RESULTS AND DISCUSSIONS

Figure 1 displays the experimental spectrum of Sc via intermediate state [Ar] $3d4s4p\ ^2F_{5/2}$ in the energy region 52 625–54 046 cm^{-1}, noted that the excitation energy is corresponding to the ground state of scandium. The spectrum spans the lowest three ionization thresholds of Sc, i.e., three fine structure states of the ground state of ionic Sc^+ $3d4s(^3D)$ [1] at 52 920–53 100 cm^{-1}. The next ionization threshold is located at 55 462.95 cm^{-1}, i.e., Sc^+ $3d4s\ ^1D_2$, it is far above 54046 cm^{-1}. Therefore, the spectrum in the energy region 52 625–53 100 cm^{-1} has numberless peaks, and there are just seven prominent peaks in the energy region 53 100–54 046 cm^{-1}.

The present paper focuses on how to classify and assign these experimental peaks. The analysis procedure is organized as follows: the spectrum is divided into three parts according to ionization thresholds, (i) below the first ionization threshold, i.e., in the energy region 52 625–52 922 cm^{-1}; (ii) between the third and first ionization threshold, i.e., in the energy region 52 922–53 040 cm^{-1}; (iii) above the third ionization threshold, i.e., in the energy region 53100–54046 cm^{-1}. We will analyze the experimental spectrum in the order of decreasing excitation energy.

A. Spectrum in the energy region 53 100–54 046 cm^{-1}

1. Experimental analysis

The experimental spectrum via intermediate state [Ar] $3d4s4p\ ^2F_{5/2}$ by two-laser resonance excitation is shown in Fig. 1. Clearly, there are seven prominent peaks with asymmetric profile in the energy region 53 100–54 046 cm^{-1}. It is well known that the asymmetric profile of an autoionization resonance arises from the interaction of bound and continuum wave functions and is often described by the Fano formula [29,30] in the simplest case, i.e., just two channels are considered:

$$\sigma(\varepsilon) = \sigma_a \frac{(q+\epsilon)^2}{1+\epsilon^2} + \sigma_b, \quad \epsilon = \frac{E - E_r}{\frac{1}{2}\Gamma}, \tag{8}$$

where E_r is the resonance energy, Γ is the natural width of the resonance, and q is called line profile index which defines the shape of a resonance. The parameters of σ_a and σ_b represent the cross sections of the continuum states that interact and do not interact with the bound state, respectively. The reduced autoionization width Γ_r is given by

$$\Gamma_r = n^{*3}\Gamma, \tag{9}$$

where $n^* = n - \mu_n$ is the effective quantum number. The reduced autoionization width is theoretically expected to be independent of n for a Rydberg or autoionization Rydberg series [32]. The Fano formula is extended to include the interaction of many resonances with many continua [31,33], i.e., the so-called Shore's parametrization [31] which includes the interaction of many resonances with many continua:

$$\sigma(E) = C + \sum_k \frac{\frac{1}{2}\Gamma_k B_k + (E - E_k)A_k}{(E-E_k)^2 + \left(\frac{\Gamma_k}{2}\right)^2}. \tag{10}$$

Since the smallest energy interval among these seven prominent peaks is much larger than the width of any resonance, it may be reasonable to fit to the experimental data with the Fano formula. Such fitting results may suggest whether a specific peak can be appropriately described by the simplest case, i.e., just two channels are considered. On the other hand, the measured profile of an autoionization resonance is result of the theoretical profile convoluted with the

TABLE I. The fitted Fano parameters E_r, q, Γ, Γ_r as well as the effective quantum number n^*.

Peak	E_r (cm^{-1})	n^* [a]	q	Γ (cm^{-1})	$\Gamma_r=n^{*3}\Gamma$
a_1	53213.72	6.98	−4.41	0.73	248.25
a_2	53719.25	7.93	−25.91	0.17	84.88
b_1	53315.78	7.15	2.99	22.41	8191.43
b_2	53770.69	8.05	7.74	0.92	479.93
c_1	53435.34	7.36	4.10	12.61	5027.46
c_2	53836.45	8.21	4.46	10.42	5766.30
d	53493.05	3.25/5.09	2.48	12.00	411.94/1573.14

[a] n^* is obtained from experimental energy levels with the ionization threshold Sc^+ $3d4s$ $^1D_2$ 55 462.95 cm^{-1} except that the ionization threshold is taken as Sc^+ $3d^2$ $^3F_2$ 57 724.87 cm^{-1} or $3d^2$ $^1D_2$ 63 866.56 cm^{-1} for the peak d.

instrumental function $F(E)$, which can be approximated by Gaussian profile with the full width at half maximum (FWHM) 0.5 cm^{-1} in this experiment. Therefore, an experimental autoionization state is fitted by the profile of the Fano formula convoluted with a Gaussian profile with the FWHM 0.5 cm^{-1}, except that the peak a_2 is fitted by the Fano formula due to its narrow FWHM 0.17 cm^{-1} shown in Table I. Moreover, such fitting may suggest which peak cannot be described by the simplest case, i.e., just two channels are considered. Here we take b_1 peak as an example shown in Fig. 2(a); the fitted curve agrees well with the experimental data except for the red wing of the b_1 peak, there is an evident dip in the experimental spectrum, but the fitted curve cannot reconstruct the dip. We will discuss the reason later. Table I gives the fitted Fano parameters E_r, q, and Γ. Clearly, each pair of peaks (a_1,a_2), (b_1,b_2), and (c_1,c_2) have similar quantum defects μ, therefore, these peaks can be classified into three pairs of peaks (a_1,a_2), (b_1,b_2), and (c_1,c_2) as well as one isolated peak d, and (a_1,a_2), (b_1,b_2), and (c_1,c_2) may be related to autoionization states converging to Sc^+ $3d4s$ $^1D_2$, and d may be related to an autoionization state converging to $3d^2$ $^3F_2$ and/or $3d^2$ $^1D_2$. As discussed above,

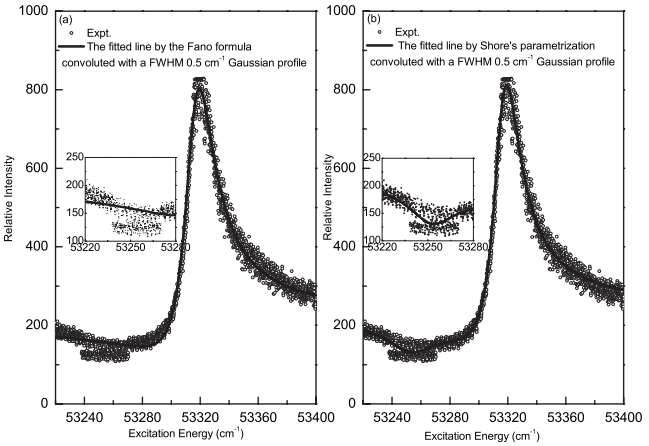

FIG. 2. (a) The b_1 peak is fitted by the Fano formula Eq. (8); (b) the b_1 peak is fitted by Shores parametrization Eq. (10) in which two resonances are included. The inset in both (a) and (b) displays the expand view in the energy region 53 220–53 280 cm^{-1}.

along a Rydberg or autoionization Rydberg series, the reduced autoionization width Γ_r is theoretically expected to be independent of n. However, as shown in Table I, except that the pair of peaks (c_1,c_2) has the nearly constant Γ_r, Γ_r vary dramatically in pairs of (a_1,a_2) and (b_1,b_2). More specifically, the Γ_r ratio of a_1 to a_2 is about three, while there is an order-of-magnitude variation for Γ_r in pairs of (b_1,b_2). For the case of the pair of peaks (a_1,a_2), it may be due to the very narrow width of a_2 peak. The reason that the apparent width of a_2 peak is much smaller than the FWHM of the laser employed in this experiment may result from the noncoherent superposition of two closely spaced autoionization states. We will give further discussion about the phenomena as well as its application in another paper. The explanation that variation for Γ_r in a pair of peaks (b_1,b_2) will need the help of theoretical analysis and will be discussed later.

2. Assignments by calculated results

To assign one specific peak needs the help of the theoretical analysis, although one may classify the experimental peaks in terms of energy position as the above analysis. Meanwhile, the theoretical analysis may give the reason that variation for Γ_r in pair of peaks (b_1,b_2).

As discussed in Sec. II, through comparing the experimental spectrum with a specific eigenchannel spectrum in terms of energy position, one may assign experimental peaks. Since the experimental spectrum of Sc is obtained by two-laser resonance excitation via intermediate state [Ar] $3d4s4p$ $^2F_{5/2}$, therefore, channels in $J^\pi=(3/2)^+,(5/2)^+,(7/2)^+$ symmetry should be considered in the calculations due to the selection rules, and the channels entered in this calculations are listed in Table II. We will assign three pairs of peaks (a_1,a_2), (b_1,b_2), and (c_1,c_2) as well as one isolated peak d one by one.

Figure 3(a) shows the calculated eigenchannel spectrum related to autoionization Rydberg series $3d4s(^1D_2)nd_{3/2}$, $J^\pi=(3/2)^+$. Clearly, in the eigenchannel spectrum, there are two prominent peaks close to the energy positions of peaks a_1 and a_2, respectively. Therefore, the pair of peaks (a_1,a_2) may be related to eigenchannel $3d4s(^1D_2)nd_{3/2}$, $J^\pi=(3/2)^+$. The principal quantum number n can be deduced from the experimental energy level $3d4s(^1D_2)nd_{3/2}$, $J^\pi=(3/2)^+$ (energy level

TABLE II. Dissociation channels included in the present calculations.

$J^\pi=(3/2)^+$	$J^\pi=(5/2)^+$	$J^\pi=(7/2)^+$
$3d4s(^3D_1)\varepsilon d_{3/2}$	$3d4s(^3D_1)\varepsilon d_{3/2}$	$3d4s(^3D_1)\varepsilon d_{5/2}$
$3d4s(^3D_1)\varepsilon d_{5/2}$	$3d4s(^3D_1)\varepsilon d_{5/2}$	$3d4s(^3D_2)\varepsilon d_{3/2}$
$3d4s(^3D_1)\varepsilon s_{1/2}$	$3d4s(^3D_2)\varepsilon s_{1/2}$	$3d4s(^3D_2)\varepsilon d_{5/2}$
$3d4s(^3D_2)\varepsilon d_{3/2}$	$3d4s(^3D_2)\varepsilon d_{3/2}$	$3d4s(^3D_3)\varepsilon s_{1/2}$
$3d4s(^3D_2)\varepsilon d_{5/2}$	$3d4s(^3D_2)\varepsilon d_{5/2}$	$3d4s(^3D_3)\varepsilon d_{3/2}$
$3d4s(^3D_2)\varepsilon s_{1/2}$	$3d4s(^3D_3)\varepsilon s_{1/2}$	$3d4s(^3D_3)\varepsilon d_{5/2}$
$3d4s(^1D_2)\varepsilon d_{3/2}$	$3d4s(^3D_3)\varepsilon d_{3/2}$	$3d4s(^1D_2)\varepsilon d_{3/2}$
$3d4s(^3D_3)\varepsilon d_{3/2}$	$3d4s(^3D_3)\varepsilon d_{5/2}$	$3d4s(^1D_2)\varepsilon d_{5/2}$
$3d4s(^3D_3)\varepsilon d_{5/2}$	$3d4s(^1D_2)\varepsilon s_{1/2}$	$3d^2(^3F_2)\varepsilon d_{3/2}$
$3d4s(^1D_2)\varepsilon d_{5/2}$	$3d4s(^1D_2)\varepsilon d_{3/2}$	$3d^2(^3F_2)\varepsilon d_{5/2}$
$3d4s(^1D_2)\varepsilon s_{1/2}$	$3d4s(^1D_2)\varepsilon d_{5/2}$	$3d^2(^3F_3)\varepsilon s_{1/2}$
$3d^2(^3F_2)\varepsilon s_{1/2}$	$3d^2(^3F_2)\varepsilon s_{1/2}$	$3d^2(^3F_3)\varepsilon d_{3/2}$
$3d^2(^3F_2)\varepsilon d_{3/2}$	$3d^2(^3F_2)\varepsilon d_{3/2}$	$3d^2(^3F_3)\varepsilon d_{5/2}$
$3d^2(^3F_2)\varepsilon d_{5/2}$	$3d^2(^3F_2)\varepsilon d_{5/2}$	$3d^2(^3F_4)\varepsilon s_{1/2}$
$3d^2(^3F_3)\varepsilon d_{3/2}$	$3d^2(^3F_3)\varepsilon s_{1/2}$	$3d^2(^3F_4)\varepsilon d_{3/2}$
$3d^2(^3F_3)\varepsilon d_{5/2}$	$3d^2(^3F_3)\varepsilon d_{3/2}$	$3d^2(^3F_4)\varepsilon d_{5/2}$
$3d^2(^3F_4)\varepsilon d_{5/2}$	$3d^2(^3F_3)\varepsilon d_{5/2}$	$3d^2(^1D_2)\varepsilon d_{3/2}$
$3d^2(^1D_2)\varepsilon s_{1/2}$	$3d^2(^3F_4)\varepsilon d_{3/2}$	$3d^2(^1D_2)\varepsilon d_{5/2}$
$3d^2(^1D_2)\varepsilon d_{3/2}$	$3d^2(^3F_4)\varepsilon d_{5/2}$	$3d^2(^3P_0)\varepsilon d_{5/2}$
$3d^2(^1D_2)\varepsilon d_{5/2}$	$3d^2(^1D_2)\varepsilon s_{1/2}$	$3d^2(^3P_1)\varepsilon d_{3/2}$
$4s^2(^1S_0)\varepsilon d_{3/2}$	$3d^2(^1D_2)\varepsilon d_{3/2}$	$3d^2(^3P_1)\varepsilon d_{5/2}$
$3d^2(^3P_0)\varepsilon d_{3/2}$	$3d^2(^1D_2)\varepsilon d_{5/2}$	$3d^2(^1G_4)\varepsilon s_{1/2}$
$3d^2(^3P_1)\varepsilon s_{1/2}$	$4s^2(^1S_0)\varepsilon d_{5/2}$	$3d^2(^1G_4)\varepsilon d_{3/2}$
$3d^2(^3P_1)\varepsilon d_{3/2}$	$3d^2(^3P_0)\varepsilon d_{5/2}$	$3d^2(^1G_4)\varepsilon d_{5/2}$
$3d^2(^3P_1)\varepsilon d_{5/2}$	$3d^2(^3P_1)\varepsilon d_{3/2}$	
$3d^2(^3P_2)\varepsilon s_{1/2}$	$3d^2(^3P_1)\varepsilon d_{5/2}$	
$3d^2(^3P_2)\varepsilon d_{3/2}$	$3d^2(^3P_2)\varepsilon s_{1/2}$	
$3d^2(^3P_2)\varepsilon d_{5/2}$	$3d^2(^3P_2)\varepsilon d_{3/2}$	
$3d^2(^1G_4)\varepsilon d_{5/2}$	$3d^2(^3P_2)\varepsilon d_{5/2}$	
$3d^2(^1S_0)\varepsilon d_{3/2}$	$3d^2(^1G_4)\varepsilon d_{3/2}$	
	$3d^2(^1G_4)\varepsilon d_{5/2}$	
	$3d^2(^1S_0)\varepsilon d_{5/2}$	

is 43 466.39 cm^{-1}, $n^*=3.02$) [1]. Thus, a_1 and a_2 may be assigned as $3d4s(^1D_2)8d_{3/2}$, $J^\pi=(3/2)^+$ ($n^*=6.98$) and $3d4s(^1D_2)9d_{3/2}$, $J^\pi=(3/2)^+$ ($n^*=7.93$). The difference between experimental and calculated quantum defects for the pair of peaks (a_1,a_2) is about 0.04 as shown in Table III. Noted that there are also some small peaks in the calculated eigenchannel spectrum as shown in Fig. 3(a), it is due to configuration interaction among these autoionization Rydberg series converging to different levels of Sc^+. In addition, channels with $J^\pi=(5/2)^+,(7/2)^+$ symmetry have no contribution to the pair of peaks (a_1,a_2) based on our calculations.

Now we discuss the assignments for the pair of peaks (b_1,b_2); Fig. 4 shows the calculated eigenchannel spectrum related to the pair of peaks (b_1,b_2). As for the $J^\pi=(5/2)^+$ symmetry, both the calculated eigenchannel spectrum related to autoionization Rydberg series $3d4s(^1D_2)nd_{5/2}$ and related to autoionization Rydberg series $3d4s(^1D_2)nd_{3/2}$ have two

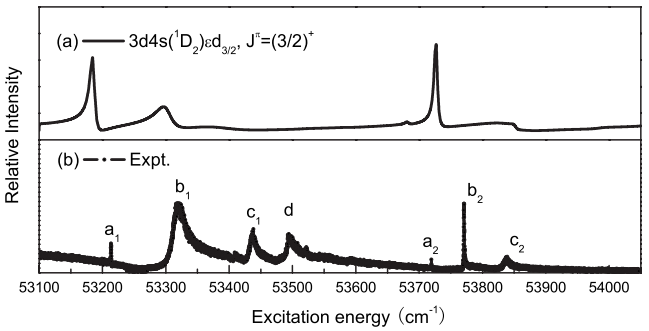

FIG. 3. Comparison of the present calculated eigenchannel spectra with the experimental spectrum of Sc via intermediate state Sc [Ar] $3d4s4p\ ^2F_{5/2}$ in the energy region 53 100–54 046 cm^{-1}: (a) the calculated eigenchannel spectrum for channel $3d4s(^1D_2)\varepsilon d_{3/2}$ in $J^\pi=(3/2)^+$ symmetry; (b) the experimental spectrum.

prominent peaks close to the pair of peaks (b_1,b_2), as shown in Figs. 4(a) and 4(b), respectively. Therefore, the pair of peaks (b_1,b_2) may be assigned as $[3d4s(^1D_2)8d_{5/2}$, $J^\pi=(5/2)^+$ ($n^*=7.16$), $3d4s(^1D_2)9d_{5/2}$, $J^\pi=(5/2)^+$ ($n^*=8.05$)], and/or $[3d4s(^1D_2)8d_{3/2}$, $J^\pi=(5/2)^+$ ($n^*=7.16$), $3d4s(^1D_2)9d_{3/2}$, $J^\pi=(5/2)^+$ ($n^*=8.05$)]. The principal quantum number n can be deduced from the experimental energy level $3d4s(^1D_2)4d$, $J^\pi=(5/2)^+$ (energy level is 42 445.55 cm^{-1}, $n^*=2.90$) [1] and/or $3d4s(^1D_2)4d$, $J^\pi=(5/2)^+$ (energy level is 42 149.66 cm^{-1}, $n^*=2.87$) [1]. Noted that the prominent peak around peak d in the calculated eigenchannel spectrum for $3d4s(^1D_2)\varepsilon d_{3/2}$, $J^\pi=(5/2)^+$ mainly results from the configuration interaction between eigenchannel of $3d4s(^1D_2)\varepsilon d_{3/2}$, $J^\pi=(5/2)^+$ and eigenchannel of $3d^2(^1D_2)\varepsilon d_{3/2}$, $J^\pi=(5/2)^+$ shown in Fig. 6(b). Meanwhile, as for the $J^\pi=(7/2)^+$ symmetry, the calculated eigenchannel spectrum related to autoionization Rydberg series $3d4s(^1D_2)nd_{5/2}$ has two prominent peaks close to the pair of peaks (b_1,b_2), as shown in Fig. 4(d). Therefore, the pair of peaks (b_1,b_2) may also be assigned as $[3d4s(^1D_2)8d_{5/2}$, $J^\pi=(7/2)^+$ ($n^*=7.16$), $3d4s(^1D_2)9d_{5/2}$, $J^\pi=(7/2)^+$ ($n^*=8.05$)]. The principal quantum number n can be deduced from the experimental energy level $3d4s(^1D_2)4d$, $J^\pi=(7/2)^+$ (energy level is 42 198.84 cm^{-1}, $n^*=2.88$) [1]. Furthermore, there are two peaks labeled as b_{1a} and b_{1b} close to b_1 peak in the calculated eigenchannel spectrum $3d4s(^1D_2)\varepsilon d_{5/2}$, $J^\pi=(7/2)^+$ shown in Fig. 4(d), which may come from configuration interaction with other channels of autoionization Rydberg series. In fact, b_{1a} may come from configuration interaction between $3d4s(^1D_2)\varepsilon d_{5/2}$, $J^\pi=(7/2)^+$ and $3d4s(^1D_2)nd_{3/2}$, $J^\pi=(7/2)^+$, and b_{1b} come from configuration interaction between $3d4s(^1D_2)\varepsilon d_{5/2}$, $J^\pi=(7/2)^+$ and $3d^2(^1D_2)nd_{5/2}$, $J^\pi=(7/2)^+$, which can be shown in Figs. 4(e) and 4(f), respectively. Furthermore, the evident dip at the red wing of b_1 peak may result from the contribution from the peak b_{1a} close to b_1 related to autoionization Rydberg series $3d4s(^1D_2)nd_{3/2}$, $J^\pi=(7/2)^+$, and the much broader width of b_1 which result in an order-of-magnitude variation for Γ_r in pairs of (b_1,b_2) may be due to the contribution from the peak b_{1b} which is close to b_1 and related to autoionization Rydberg series $3d^2(^1D_2)nd_{5/2}$, $J^\pi=(7/2)^+$. Therefore, we fit the experimental spectrum around b_1 with the Shore's parametri-

TABLE III. Comparison of energy positions (cm^{-1}) between the present calculated and experimental autoionization states in the 53 100–54 046 cm^{-1} energy region.

Expt.			Theor.			
Peak	E_r	n^*	E_{theor}	$\Delta\mu$ [a]	Assignment	J^π
a_1	53213.83	6.99	53183.29	0.04	$3d4s(^1D_2)8d_{3/2}$	$\frac{3}{2}^+$
a_2	53719.25	7.93	53726.00	−0.02	$3d4s(^1D_2)9d_{3/2}$	$\frac{3}{2}^+$
b_1	53315.81	7.15	53309.57	0.01	$3d4s(^1D_2)8d_{3/2}$	$\frac{5}{2}^+$
			53314.99	0.01	$3d4s(^1D_2)8d_{5/2}$	$\frac{5}{2}^+$
			53304.39	0.02	$3d4s(^1D_2)8d_{5/2}$	$\frac{7}{2}^+$
b_2	53770.87	8.05	53814.36	−0.10	$3d4s(^1D_2)9d_{3/2}$	$\frac{5}{2}^+$
			53806.24	−0.09	$3d4s(^1D_2)9d_{5/2}$	$\frac{5}{2}^+$
			53801.50	−0.09	$3d4s(^1D_2)9d_{5/2}$	$\frac{7}{2}^+$
c_1	53436.14	7.36	53402.21	0.06	$3d4s(^1D_2)8d_{5/2}$	$\frac{3}{2}^+$
c_2	53836.78	8.21	53855.38	−0.05	$3d4s(^1D_2)9d_{5/2}$	$\frac{3}{2}^+$
d	53493.06	3.25	53502.06	0.00	$3d^2(^1D_2)4d_{3/2}$	$\frac{5}{2}^+$
		5.09	53511.35	−0.01	$3d^2(^3F_2)6d_{5/2}$	$\frac{7}{2}^+$

[a] $\Delta\mu=\mu_{expt.}-\mu_{theor.}$

zation, in which two resonances are included due to that b_{1b} peak can not be identified from the broad peak b_1. The fitted result is shown in Fig. 2(b); certainly, the evident dip at the red wing of b_1 peak is well reconstructed.

Table III shows the summary of assignments for the pair of peaks (b_1,b_2), the calculated energy positions. The difference between experimental and calculated quantum defects for the peak b_1 is about 0.01–0.02, while it is about 0.09–0.10 for the peak b_2. However, as shown in Fig. 4 and Table III, the calculated accuracy is sufficient to assign the peak b_2 even for the largest quantum defect error 0.10.

Similarly, Fig. 5 shows the calculated eigenchannel spectrum related to the pair of peaks (c_1,c_2). Table I shows that the pair of peaks (c_1,c_2) has the nearly constant Γ_r; in fact, the pair of peaks (c_1,c_2) is simply related to autoionization Rydberg series $3d4s(^1D_2)nd_{5/2}$, $J^\pi=(3/2)^+$ as shown in Fig. 5(a). Therefore, c_1 and c_2 are assigned as $3d4s(^1D_2)8d_{5/2}$, $J^\pi=(3/2)^+$ $(n^\star=7.36)$ and $3d4s(^1D_2)9d_{5/2}$, $J^\pi=(3/2)^+$ $(n^\star=8.22)$. The principal quantum numbers are deduced according to experimental energy level $3d4s(^1D_2)4d_{5/2}$, $J=(3/2)^+$ (energy level is 42 446.39 cm^{-1}, $n^\star=2.91$) [1]. The difference between experimental and calculated quantum defects for the pair of peaks (c_1,c_2) is not larger than 0.06.

As for the assignment about the peak d, based on our calculations shown in Fig. 6, peak d is assigned as $3d^2(^3F_2)6d_{5/2}$, $J^\pi=(7/2)^+$ $(n^*=5.09)$ and/or $3d^2(^1D_2)4d_{3/2}$, $J^\pi=(5/2)^+$ $(n^*=3.25)$. The principal quantum numbers are

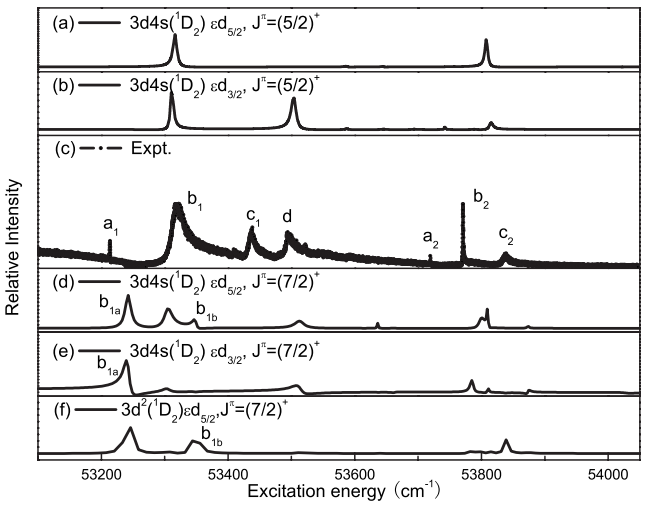

FIG. 4. Comparison of the present calculated eigenchannel spectra with the experimental spectrum of Sc via intermediate state Sc [Ar] $3d4s4p\ ^2F_{5/2}$ in the energy region 53 100–54 046 cm^{-1}: (a) the calculated eigenchannel spectrum for channel $3d4s(^1D_2)\varepsilon d_{5/2}$ $J^\pi=(5/2)^+$ symmetry; (b) the calculated eigenchannel spectrum for channel $3d4s(^1D_2)\varepsilon d_{3/2}$ in $J^\pi=(5/2)^+$ symmetry; (d) the calculated eigenchannel spectrum for channel $3d4s(^1D_2)\varepsilon d_{5/2}$ in $J^\pi=(7/2)^+$ symmetry; (e) the calculated eigenchannel spectrum for channel $3d4s(^1D_2)\varepsilon d_{3/2}$ in $J^\pi=(7/2)^+$ symmetry; (f) the calculated eigenchannel spectrum for channel $3d^2(^1D_2)\varepsilon d_{5/2}$ in $J^\pi=(7/2)^+$ symmetry; (c) the experimental spectrum.

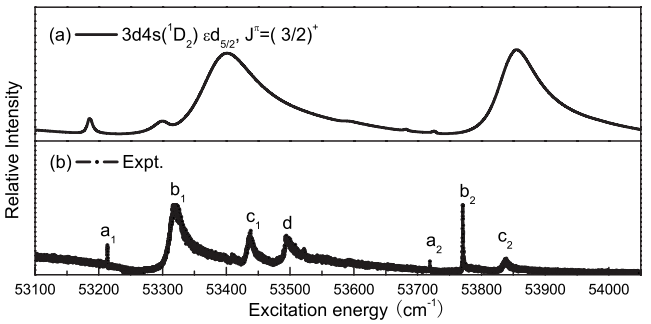

FIG. 5. Comparison of the present calculated eigenchannel spectra with the experimental spectrum of Sc via intermediate state Sc [Ar] $3d4s4p\ ^2F_{5/2}$ in the energy region 53 100–54 046 cm^{-1}: (a) the calculated eigenchannel spectrum for channel $3d4s(^1D_2)\varepsilon d_{5/2}$ in $J^\pi=(3/2)^+$ symmetry; (b) the experimental spectrum.

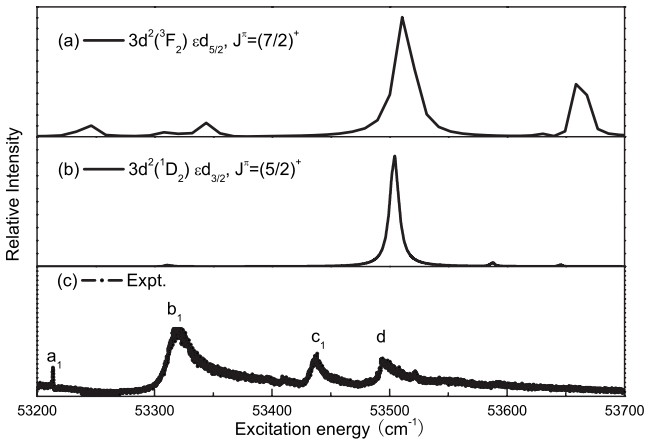

FIG. 6. Comparison of the present calculated eigenchannel spectra with the experimental spectrum of Sc via intermediate state Sc [Ar] $3d4s4p\ ^2F_{5/2}$ in the energy region 53 200–53 700 cm^{-1}: (a) the calculated eigenchannel spectrum for channel $3d^2(^3F_2)\varepsilon d_{5/2}$ in $J^\pi=(7/2)^+$ symmetry; (b) the calculated eigenchannel spectrum for channel $3d^2(^1D_2)\varepsilon d_{3/2}$ in $J^\pi=(5/2)^+$; (c) the experimental spectrum.

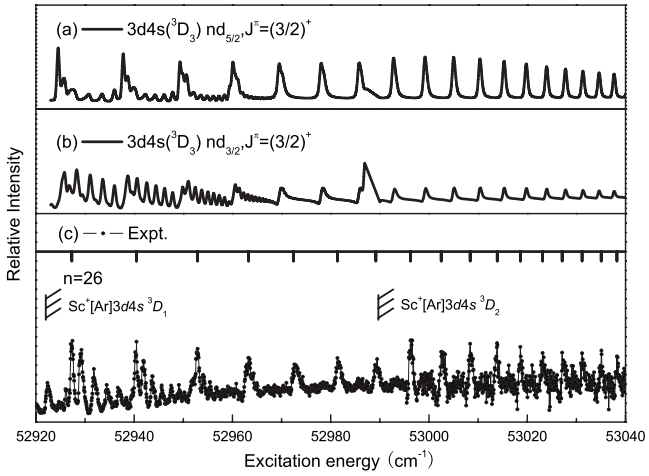

FIG. 7. Comparison of calculated eigenchannel spectra with the experimental spectrum of Sc via intermediate state Sc [Ar] $3d4s4p\ ^2F_{5/2}$ in the energy region 52 920–53 040 cm^{-1}: (a) the calculated eigenchannel spectrum for channel $3d4s(^3D_3)\varepsilon d_{5/2}$ in $J^\pi=(3/2)^+$ symmetry; (b) the calculated eigenchannel spectrum for channel $3d4s(^3D_3)\varepsilon d_{3/2}$ in $J^\pi=(3/2)^+$ symmetry; (c) the experimental spectrum.

deduced according to experimental energy level $3d^2(^3F_2)4d$, $J^\pi=(7/2)^+$ (energy level is 45 752.28 cm^{-1}, $n^*=3.03$) [1] and $3d^3$, $J=(5/2)^+$ (Energy level is 40 802.76 cm^{-1}, $n^\star=2.18$) [1]. Table III shows the summary of assignments for the peak *d*. The difference between experimental and calculated quantum defects for the peak *d* is about 0.01. Small peaks in other energy regions in the calculated spectrum for eigenchannel $3d4s(^3F_2)\varepsilon d_{5/2}$, $J^\pi=(7/2)^+$ may come from configuration interaction among autoionization Rydberg series $3d4s(^1D_2)nd_{3/2}$, $J^\pi=(7/2)^+$, $3d^2(^3F_2)nd_{5/2}$, $J^\pi=(7/2)^+$, as shown in Figs. 4(d) and 6(a), and other autoionization Rydberg series converging to higher levels of Sc^+.

B. Spectrum in the energy region 52 922–53 040 cm^{-1}

Now let us discuss the spectrum between the third and first ionization threshold 52 920–53 040 cm^{-1}. As shown in Fig. 7(c), there are much rich lines in this energy region due to the small fine structure interval of the ground state of Sc^+. It is interesting to note that there is a distinct autoionization Rydberg series converging to Sc^+ $3d4s\ ^3D_3$, which energy positions as well as the effective quantum numbers are listed in Table IV. Noted that the energy position for a specific peak belong to this autoionization Rydberg series is approximately determined by its maximum due to its symmetric profile. As for the assignment for the autoionization Rydberg series, Figs. 7(a) and 7(b) show the calculated spectrum for eigenchannel $3d4s(^3D_3)\varepsilon d_{5/2}$, $J^\pi=(3/2)^+$ and/or $3d4s(^3D_3)\varepsilon d_{3/2}$, $J^\pi=(3/2)^+$, respectively. Clearly, both of them generally agree with the experimental spectrum in the energy region 52 920–53 040 cm^{-1}. The difference between experimental and calculated energy positions is in the range of 1.47–3.76 cm^{-1}. Therefore, this autoionization Rydberg series may mainly be related to channel $3d4s(^3D_3)nd_{5/2}$, $J^\pi=(3/2)^+$ and/or $3d4s(^3D_3)n_{3/2}$, $J^\pi=(3/2)^+$ ($n=26$–43). The principal quantum numbers are deduced according to experimental energy level $3d4s(^3D_3)5d$, $J^\pi=(3/2)^+$ (energy level is 46 329.23 cm^{-1}, $n^*=4.03$) [1]. However, there are some other closely spaced peaks around the states of $n=26$, 27, and 28 in the experimental spectrum; it may be interference patterns resulting from configuration interaction among different autoionization Rydberg series converging to the same ionization threshold $3d4s(^3D_3)$. The calculated eigenchannel spectrum also reconstructs the phenomenon as shown in Figs. 7(a) and 7(b). Such strong wave function mixing makes assignment meaningless, thus, it cannot be treated seriously which peak corresponds to $n=26$, 27 and 28, respectively. We just select the strongest peak and list them in Table IV.

C. Spectrum in the energy region 52 625–52 922 cm^{-1}

Finally, we discuss the spectrum below the first ionization threshold 52 625–52 922 cm^{-1}, there are rich peaks. It is reasonable to deduce that the distinct autoionization Rydberg series converging to Sc^+ $3d4s\ ^3D_3$ observed in experimental spectra above the first ionization threshold should have some lower *n* states with strong intensity observed in this energy region. In fact, as shown in Fig. 8 and Table IV, some strong peaks are assigned as the states belonging to this autoionization Rydberg series in terms of energy position and intensity. The difference between experimental and calculated energy positions is in the range of −3.96–2.77 cm^{-1}. As for other peaks, most of them are overlapped due to the small fine structure interval for the ground state of Sc^+ and the linewidth 0.5 cm^{-1} of the laser employed in this experiment. It is difficult to assign most of these peaks due to the accuracy of our calculations, because the error in the quantum defect increases rapidly as *n* gets large even if there is a small error in energy level $[\Delta\mu=\Delta E(n-\mu)^3]$ and the principal quantum numbers *n* is larger than 21 for the Rydberg series converging to $3s4d\ ^3D_1$ in this energy region.

TABLE IV. Comparison of energy positions (cm^{-1}) between the present calculated and experimental autoionization Rydberg series in the energy region 52 625–53 040 cm^{-1}.

Expt.		Theor.	
$E_{Expt.}$ (cm^{-1})	n^* [a]	$3d4s(^3D_3)nd_{5/2}$, $J^\pi=\frac{3}{2}^+$	$3d4s(^3D_3)nd_{3/2}$, $J^\pi=\frac{3}{2}^+$
52726.94	17.16	52724.17	52727.84
52768.58	18.20	52766.47	52769.01
52804.99	19.29	52804.16	52805.07
52831.56	20.23	52829.83	52830.44
52855.65	21.20	52853.94	52855.15
52877.62	22.23	52876.34	52881.55
52896.92	23.26	52896.57	52897.76
52912.64	24.22	52912.69	52911.98
52927.31	25.23	52924.50	52925.83
52940.48	26.25	52937.75	52938.70
52952.91	27.34	52949.25	52949.92
52963.27	28.35	52960.01	52960.90
52972.41	29.35	52969.56	52969.90
52981.36	30.44	52978.13	52978.44
52989.18	31.50	52985.75	52986.96
52996.23	32.56	52992.73	52992.96
53002.47	33.58	52999.18	52999.37
53008.37	34.65	53004.97	53005.08
53013.87	35.74	53010.38	53010.40
53018.61	36.77	53015.25	53015.30
53023.13	37.84	53019.82	53019.93
53027.10	38.86	53023.95	53024.03
53031.16	40.00	53027.84	53027.77
53035.06	41.18	53031.30	53031.35
53038.24	42.23	53034.64	53034.67

[a] n^* is obtained from experimental energy levels with the ionization threshold Sc^+ $3d4s\ ^3D_3$ 53 099.76 cm^{-1}.

Based on work above, we have provided clear assignments the experimental spectrum of Sc via intermediate state $3d4s4p\ ^2F_{5/2}$, and determined the eigenchannels that give primary contribution to such experimental spectrum. It is interesting that all of these autoionization Rydberg series are related to $3d4snd_{3/2,5/2}$; it is understandable that the experimental spectrum results from the transition from the intermediate state $3d4s4p\ ^2F_{5/2}$. Based on these assignments, D_α can be obtained by comparing with experimental data by Eq. (7) and shown in Table V. Therefore, we can reconstruct spectrum above the first ionization threshold by Eq. (7) with the calculated μ_α, the calculated $U_{i\alpha}$, and the fitted D_α. The calculated spectrum is in general agreement with the experimental spectrum as shown in Fig. 9. Noted that only the eigenchannels that give primary contribution to such experimental spectrum are considered in procedure of determining the value D_α, the omitted eigenchannels may affect the profile in certain energy regions. But the present work should meet the purpose of assignment.

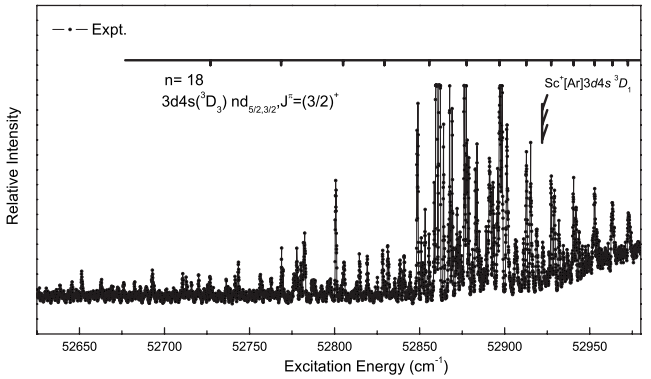

FIG. 8. Experimental spectrum of Sc Rydberg and autoionization states via intermediate state Sc [Ar] $3d4s4p\ ^2F_{5/2}$ in the energy region 52 625–52 980 cm^{-1}.

IV. CONCLUSIONS

In summary, the experimental spectrum of Sc via intermediate state $3d4s4p\ ^2F_{5/2}$ in the energy region 52 625–54 046 cm^{-1} has been obtained by two-laser resonance excitation and shown in Fig. 1. There is a distinct autoionization Rydberg series observed in the energy region 52 922–53 040 cm^{-1} and seven prominent peaks observed in the energy region 53 100–54 046 cm^{-1}. The seven prominent peaks can be classified into three pairs of peaks (a_1,a_2),

TABLE V. Eigenchannels included in constructing the calculated spectra and the corresponding dipole matrix elements D_α of the eigenchannels. D_α is obtained by fitting with the experimental spectra.

$J^\pi=(3/2)^+$		$J^\pi=(5/2)^+$		$J^\pi=(7/2)^+$	
Channels	D_α	Channels	D_α	Channels	D_α
$3d4s(^3D_3)\varepsilon d_{3/2}$	−0.5	$3d4s(^3D_2)\varepsilon d_{3/2}$	0.5	$3d4s(^3D_2)\varepsilon d_{5/2}$	1.0
$3d4s(^3D_3)\varepsilon d_{5/2}$	−0.5	$3d4s(^3D_2)\varepsilon d_{5/2}$	0.5	$3d4s(^3D_3)\varepsilon d_{3/2}$	1.0
$3d4s(^1D_2)\varepsilon d_{3/2}$	1.0	$3d4s(^3D_3)\varepsilon d_{3/2}$	0.1	$3d4s(^1D_2)\varepsilon d_{3/2}$	1.0
$3d4s(^1D_2)\varepsilon d_{5/2}$	1.0	$3d4s(^3D_3)\varepsilon d_{5/2}$	0.1	$3d4s(^1D_2)\varepsilon d_{5/2}$	2.0
$3d^2(^3F_4)\varepsilon d_{5/2}$	−0.05	$3d4s(^1D_2)\varepsilon d_{3/2}$	2.0	$3d^2(^3F_2)\varepsilon d_{5/2}$	0.5
$3d^2(^3P_2)\varepsilon d_{3/2}$	0.1	$3d4s(^1D_2)\varepsilon d_{5/2}$	1.0	$3d^2(^1D_2)\varepsilon d_{5/2}$	−1.0
$3d^2(^3P_2)\varepsilon d_{5/2}$	0.05	$3d^2(^1D_2)\varepsilon d_{3/2}$	−0.1		

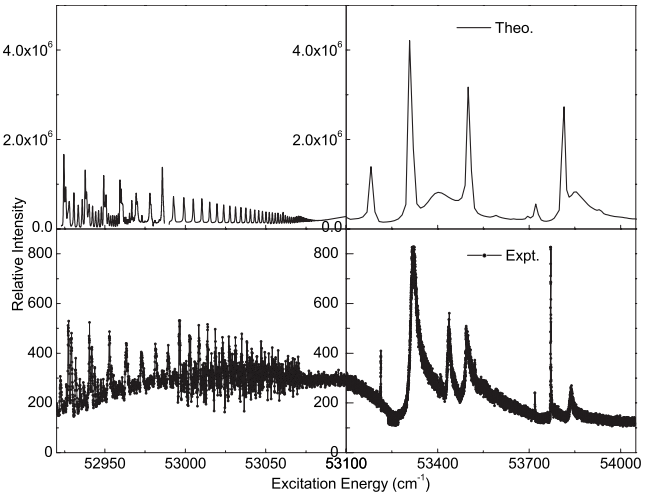

FIG. 9. Comparison of the present calculated spectrum (upper figure) with the experimental spectrum (lower figure) of Sc via the intermediate state Sc [Ar] $3d4s4p\ ^2F_{5/2}$ in the energy region 52 922–54 046 cm^{-1}.

(b_1,b_2), and (c_1,c_2) as well as one isolated peak d, the Fano parameters E_r, q, and Γ for these peaks are fitted shown in Table I. Meanwhile, eigenquantum defects μ_α and transformation matrices $U_{i\alpha}$ are calculated from first principles by relativistic multichannel theory within the framework of multichannel quantum defect theory. Through comparing calculated eigenchannel spectrum with the experimental spectrum, the distinct autoionization Rydberg series observed in the energy region 52 922–53 040 cm^{-1} is related to $3d4s(^3D_3)nd_{5/2}$, $J^\pi=(3/2)^+$ and/or $3d4s(^3D_3)nd_{3/2}$, $J^\pi=(3/2)^+$, $(n=26-43)$, as shown in Fig. 7 and Table IV. Also the three pairs of peaks (a_1,a_2), (b_1,b_2), and (c_1,c_2) are corresponding to three autoionization Rydberg converging to $3d4s\ ^1D_2$ as well as the peak d related to autoionization Rydberg converging to $3d^2\ ^1D_2$ and/or $3d^2\ ^3F_2$, such comparisons are shown in Figs. 3–6 and corresponding assignments are summarized in Table III. Generally, our calculations agree with the experimental spectrum. Furthermore, the variation for Γ_r in pair of peaks (b_1,b_2) is due to the fact that more than one resonance is included around peak b_1. Finally, based on the above assignments, D_α are obtained by comparing with experimental data and shown in Table V. With the calculated μ_α, the calculated $U_{i\alpha}$ and the fitted D_α, the spectrum above the first ionization threshold is reconstructed by Eq. (7) and shown in Fig. 9. The calculated spectrum is in general agreement with the experimental spectrum as a whole.

ACKNOWLEDGMENTS

This work was supported by the National Natural Science Foundation of China under Grants No. 10574162 and No. 10676014. The authors are deeply grateful to Professor Jia-Ming Li for helpful discussions.

[1] Yu. Ralchenko, A. E. Kramida, J. Reader, and NIST ASD Team, NIST Atomic Spectra Database (version 3.1.5), 2008, available: http://physics.nist.gov/asd3, National Institute of Standards and Technology, Gaithersburg, MD.
[2] F. Robicheaux and C. H. Greene, Phys. Rev. A **48**, 4429 (1993); F. Robicheaux and C. H. Greene, *ibid.* **48**, 4441 (1993).
[3] J. Ding, Q. H. Yang, Z. F. Tang, J. Xu, and L. B. Su, Acta Phys. Sin. **56**, 2207 (2007).
[4] Zh. Jin, Q. H. Nie, T. F. Xu, X. D. Sh, X. Shen, and X. H. Zhang, Acta Phys. Sin. **56**, 2261 (2007).
[5] W. R. S. Garton, E. M. Reeves, F. S. Tomkins, and B. Ercoli, Proc. R. Soc. London, Ser. A **333**, 1 (1973).
[6] F. Robicheaux and C. H. Greene, Phys. Rev. A **47**, 4908 (1993).
[7] C. H. Greene and M. Aymar, Phys. Rev. A **44**, 1773 (1991) and references therein.
[8] A. R. P. Rau and U. Fano, Phys. Rev. A **4**, 1751 (1971).
[9] C. M. Lee, J. M. Li, and K. T. Lu, Phys. Rev. A **8**, 1241 (1973).
[10] F. D. Jia, J. Y. Wang, and Zh. P. Zhong, Chin. Phys. B **17**, 2027 (2008).
[11] X. F. Zhang, S. L. Fan, F. D. Jia *et al.* (unpublished).
[12] W. Huang, X. Y. Xu, C. B. Xu, M. Xue, and D. Y. Chen, J. Opt. Soc. Am. B **12**, 961 (1995).
[13] W. R. Johnson, C. D. Lin, K. T. Cheng, and C. M. Lee, Phys. Scr. **21**, 409 (1980).
[14] U. Fano, Phys. Rev. A **2**, 353 (1970).
[15] M. J. Seaton, Rep. Prog. Phys. **46**, 167 (1983).
[16] C. Greene, U. Fano, and G. Strinati, Phys. Rev. A **19**, 1485 (1979).
[17] J. M. Li, Acta Phys. Sin. **29**, 419 (1980).
[18] J. M. Li, Acta Phys. Sin. **32**, 84 (1983).
[19] M. Aymar, Phys. Rep. **110**, 163 (1984).
[20] Y. Zou, X. M. Tong, and J. M. Li, Acta Phys. Sin. **44**, 50 (1995).
[21] W. Huang, Y. Zou, X. M. Tong, and J. M. Li, Phys. Rev. A **52**, 2770 (1995).
[22] J. M. Li, Y. J. Wu, and R. H. Pratt, Phys. Rev. A **40**, 3036 (1989).
[23] J. Yan, P. H. Zhang, X. M. Tong, and J. M. Li, Acta Phys. Sin. **45**, 1978 (1996).
[24] D. Xia and J. M. Li, Chin. Phys. Lett. **18**, 1334 (2001).
[25] D. Xia, S. Z. Zhang, Y. L. Peng, and J. M. Li, Chin. Phys. Lett. **20**, 56 (2003).
[26] C. M. Lee, Phys. Rev. A **10**, 584 (1974).
[27] J. Y. Wang, Zh. P. Zhong, F. D. Jia, Y. Zh. Qu, and Y. P. Zhong, J. Phys. B **41**, 085002 (2008).
[28] Y. P. Zhong, F. D. Jia, and Z. P. Zhong, Chin. Phys. B (to be published).
[29] U. Fano, Phys. Rev. **124**, 1866 (1961).
[30] U. Fano and J. W. Cooper, Phys. Rev. **137**, A1364 (1965).
[31] B. W. Shore, Phys. Rev. **171**, 43 (1968).
[32] J. Berkowitz, *Photoabsorption, Photoionization, and Photoelectron Spectroscopy* (Academic, New York, 1979).
[33] F. H. Mies, Phys. Rev. **175**, 164 (1968).